A. Bayo-Salas, T. Roose, and J. Beerten, “Frequency-domain modeling and assessment of AC and DC electromagnetic stability in MMC-based VSC HVDC links,” *Proc. IEEE IECON 2018,* Washington DC, USA, 21-23 Oct 2018, pp. 6015 – 6020.

Digital Object Identifier: 10.1109/IECON.2018.8591070

URL:
https://ieeexplore.ieee.org/document/8591070

Frequency-Domain Modeling and Assessment of AC and DC Electromagnetic Stability in MMC-based VSC HVDC Links

A. Bayo-Salas, T. Roose, J. Beerten

Dept. Electrical Engineering (ESAT), Division ELECTA & EnergyVille, University of Leuven (KU Leuven), Belgium
E-mail: alejandro.bayosalas; thomas.roose; jef.beerten@esat.kuleuven.be

***Abstract*—In this paper, an analysis of electromagnetic instability is presented for Voltage Source Converter High Voltage Direct Current (VSC HVDC) systems. In recent years, the interaction between electromagnetic modes of the system and the converter dynamics has shown to give rise to instability problems in the AC network, up to the kHz range. This paper extends the analysis of the problem to the DC side and investigates to what extent similar problems can be expected in future HVDC installations.**

***Keywords*—VSC HVDC, harmonic stability, control interactions, network resonances**

I. Introduction

The integration of Voltage Source Converter High Voltage Direct Current (VSC HVDC) links in the power system has given rise to a new stability problem, currently known as harmonic or electromagnetic stability. The instability is caused by dynamic electromagnetic interactions between converter control dynamics and network resonances. The problem has shown up in different forms, both in the first offshore wind farm connected via an HVDC link using two-level converter topology [1], as well as with several HVDC connections using Modular Multilevel Converters (MMC) [2]–[4].

Capturing such dynamic interactions in simulation tools requires an accurate representation of all influencing factors for frequencies up to the kHz range [5], [6]. On the network side, the frequency-dependency of passive components such as cables and overhead lines has to be accurately represented. For the converters, it is equally important to account for the most significant dynamics in the kHz range.

In real-life examples, the instability has often been triggered by AC network topological changes, causing alterations to the resonance spectrum of the electrical system [4], [7]. The experienced instabilities appeared in the kHz range. Since existing VSC HVDC installations have until now been built as point-to-point connection, the resonance spectrum at the DC side is typically well-known and can more easily be accounted for in system design studies compared to AC systems. However, with the advent of more complex multi-terminal installations and meshed HVDC grids, with converters built by different manufacturers, it is of interest to investigate to what extent such instabilities could also be experienced at the DC side in the near future.

In the past, few studied assessed the interactions between two-level VSCs and DC resonances in a DC link [8], [9]. The focus was given to the impact of outer loops and the negative-resistive behavior caused by converter constant-power operation and, consequently, instabilities appeared in the range of very low-frequency resonances. For this reason, several fast control dynamics were neglected and conventional π cable models were used. However, the detrimental interactions occurring in the kHz range, as observed in the AC side, were neglected. This paper shows that DC stability problems can also occur at higher frequencies and details the necessary modelling to capture such effects.

This paper aims at extending high-frequency electromagnetic stability analysis to both sides of the converter. First, the converter model and control is presented. Second, the frequency-domain stability assessment based on an equivalent admittance representation is introduced, both for AC and DC side analysis, with a particular attention paid to the dead-time representation on the resulting converter dynamic response. Last, a case study of a two-terminal link is presented.

II. Modular multilevel converter

A. Averaged dynamic model

The MMC model used in this study is based on the averaged dynamic model (ADM) [10]. The circuit topology of the model is depicted in Fig. 1.

The ADM assumes ideal sorting of the submodules in the converter and neglects harmonics generated due to the modulation and non-ideal turn-on and turn-off behavior [11]. This assumption allows simplifying the submodule strings in each arm of the MMC to controllable voltage sources (Fig. 1). The voltage generated by the insertion of submodule capacitors in the upper (u) arm is represented by v_u and in the lower (l) arm by v_l. The arm inductor L_{arm} limits the switching harmonics in the arm currents i_u and i_l. The inductance and resistance of the converter transformer are represented by respectively L_{tr} and R_{tr}.

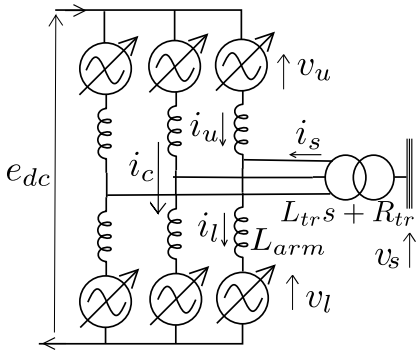

Fig. 1: MMC circuit topology.

In order to separately control DC and fundamental frequency components of the arm currents, the grid current i_s and circulating current i_c are respectively defined as

$$i_s = -i_u + i_l, \qquad i_c = \frac{i_u + i_l}{2}. \tag{1}$$

From the circuit topology of Fig. 1, the dynamics of the MMC are given by the differential equations

$$\left(L_{tr} + \frac{L_{arm}}{2}\right)\frac{d}{dt}i_s = v_s - \frac{-v_u + v_l}{2} - R_{tr}i_s, \tag{2}$$

$$L_{arm}\frac{d}{dt}i_c = \frac{e_{dc}}{2} - \frac{v_u + v_l}{2}, \tag{3}$$

where v_s is the AC phase voltage at the point of common coupling (PCC) and e_{dc} the DC side voltage.

Based on the averaging principle, the arm voltages are determined by the continuous insertion index n and the sum capacitor voltage v_c^{Σ}

$$v_u = n_u v_{c,u}^{\Sigma}, \qquad v_l = n_l v_{c,l}^{\Sigma}. \tag{4}$$

The insertion index n varies between 0 and 1, respectively representing no or all submodule capacitors inserted.

Due to the charging and discharging for the submodule capacitors during insertion, the relation between i_s, i_c and v_c^{Σ} is given by

$$\frac{C_{SM}}{N}\frac{d}{dt}v_{cu}^{\Sigma} = n_u\left(\frac{i_s}{2} + i_c\right), \tag{5}$$

$$\frac{C_{SM}}{N}\frac{d}{dt}v_{cl}^{\Sigma} = n_l\left(-\frac{i_s}{2} + i_c\right). \tag{6}$$

C_{SM} is the submodule capacitance and N the number of submodules per arm. The combination of (1)–(6) completely defines the averaged dynamic model for the MMC used in this paper.

B. MMC control structure

The overall control structure of the MMC is given in Fig. 2 and a detailed block diagram of the electrical circuit and current controllers is given in Fig 3.

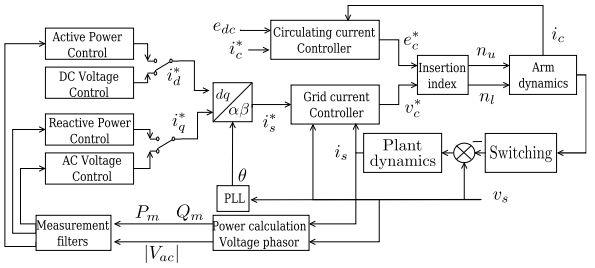

Fig. 2: MMC dynamics structure.

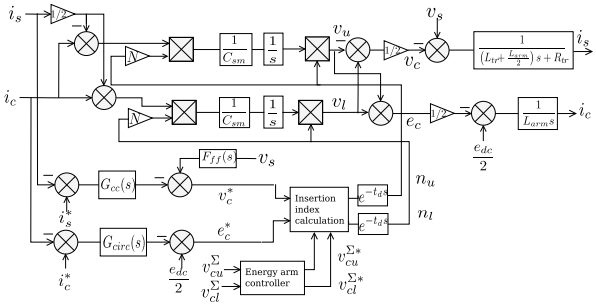

Fig. 3: MMC equivalent circuit and control diagram.

The structure is split into slow outer and the fast inner control loops. The outer loops include to the DC voltage, active/reactive power and AC voltage control and are typically characterized by a bandwidth below the fundamental frequency. To obtain the outer control reference values, PI-controllers are used. The inner controls, which largely determine the converter super-synchronous behaviour, consist of the grid current control (cc) and the circulating current control ($circ$). These two controllers are characterized by

$$v_c^* = F_{ff}(s)v_s - G_{cc}(s)\left(i_s^* - i_s\right), \tag{7}$$

$$e_c^* = \frac{e_{dc}}{2} - G_{circ}(s)\left(i_c^* - i_c\right). \tag{8}$$

The grid current controller $G_{cc}(s)$ contains the AC voltage at the PCC, v_s, as feed-forward term. This voltage is first filtered through a first-order low pass filter $F_{ff}(s)$ with a corner frequency of 350 Hz. The difference between the actual grid current i_s and the reference grid current i_s^* is controlled by $G_{cc}(s)$, a proportional-resonant (PR) controller given by

$$G_{cc}(s) = K_{ps} + \frac{K_{is}s}{s^2 + \omega_n^2}, \tag{9}$$

which is tuned to the fundamental frequency by setting ω_n equal to $2\pi 50$ rad/s. A similar control strategy is used for the circulating current control, where the DC voltage e_{dc} is used as feed-forward term and the PR-controller is represented by

$$G_{circ}(s) = K_{pc}\left(1 + \frac{K_{ic}s}{s^2 + (2\omega_n)^2}\right). \tag{10}$$

The resonant part is tuned to $2\omega_n$ to accurately track and suppress the 100 Hz-component of the circulating current [10].

The reference value of the circulating current i_c^* is given by

$$i_c^* = \frac{P_m}{3e_{dc}}, \tag{11}$$

where P_m is the active power. The output values of the grid current control, v_c^*, and circulating current control e_c^* are used to calculate the insertion indices n_u and n_l via direct modulation as

$$n_u = \frac{e_c^* - v_c^*}{e_{dc}} \qquad n_l = \frac{e_c^* + v_c^*}{e_{dc}}. \tag{12}$$

To include the effect of computational and switching delays, a time delay block is added between the calculation of the insertion indices and the application of the resulting voltage to the averaged dynamic model [12]. This time delay is exactly represented by the exponential function $e^{-t_d s}$.

The MMC parameters used in the remainder of the paper are summarized in Table I.

TABLE I: Converter parameters

Parameter	Value	Parameter	Value
AC Voltage	110 kV	*Output current control*	
DC Voltage	± 100 kV	K_{ps}	116
Base Power	150 MVA	K_{is}	5800
L_{tr}	0.069 H	*Circulating current control*	
L_{arm}	0.05 H	K_{pc}	50
R_{tr}	0.05 Ω	K_{ic}	400
C_{sm}	4 mF	*Power controller*	
N	100	K_p	0.1
		K_i	5
		DC voltage control	
Dead-time		K_p	0.006
t_d	150 μs	K_i	25

III. Stability assessment method

A. Impedance-based representation

The method for assessing the electromagnetic stability at the AC and DC side of a VSC HVDC system relies on an impedance-based representation of the converter and the respective system. In this paper, control interactions at both sides are assessed separately, focusing on the electromagnetic system characteristics of the respective subsystem (Fig. 4). The voltage v_g is the phase voltage of the AC grid. The stability at both sides can be assessed by transforming the system to a closed-loop representation with two transfer functions, respectively representing the network and the converter impact. The definition of the transfer functions of the converter, Y_{vsc}^{AC} and Y_{vsc}^{DC}, depends on the converter side of interest and is explored in more detail in the next sections.

The controls and converter dynamics as shown in Fig. 2 and 3 have been implemented in MATLAB/Simulink. The converter admittances Y_{vsc}^{AC} and Y_{vsc}^{DC} presented in this section are obtained by linearising the system at an operating point using the control toolbox.

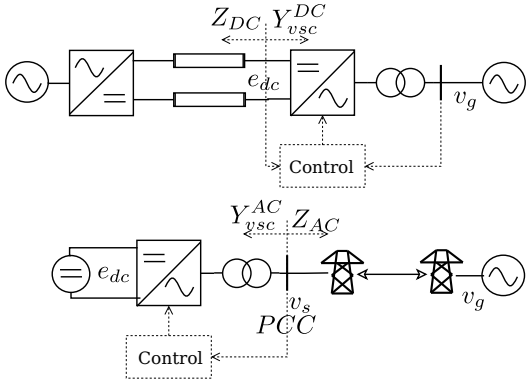

Fig. 4: Test system layout for the study of interaction at the DC side (top) and the AC side (bottom).

B. MMC equivalent admittance representation

For the analysis of electromagnetic interactions in the kHz range, particular attention is paid to the behavior of Y_{vsc}^{AC} and Y_{vsc}^{DC} above fundamental frequency. When only the passive converter components (arm inductors, transformers) are included in the analysis, the converter dynamics would be determined largely by the inductive behavior of these elements. It can thus be expected that, outside of the bandwidth of the controllers, the dynamic converter response can be approximated by the inductive behavior of these components. In absence of any control dynamics (and whilst neglecting losses), the AC side admittance would thus be completely characterized by the equivalent inductance of the connection of transformer and arm reactors, defined as $L_t = L_{tr} + L_{arm}/2$. The DC side converter admittance, Y_{vsc}^{DC} indicates how a change in the DC voltage e_{dc} affects the DC current i_{dc}. Following a similar reasoning, this admittance would, in absence of any control dynamics, be characterized by the parallel connection of the phase arm reactors as seen from the DC bus. This equivalent inductance is represented by L_{DC}.

$$L_{DC} = \frac{3}{2 \cdot L_{arm}}. \tag{13}$$

Because of the impact of control dynamics, the VSC admittance observed at both sides differs from this ideal passive behavior, shown in Fig. 5. Fig. 5a includes a comparison between an AC side equivalent admittance model where only the passive elements are considered, i.e. $1/(L_t s + R_{tr})$, and a model where both the passive elements and the converter control dynamics are included, i.e. Y_{vsc}^{AC}. It is clear that the converter admittance indeed behaves asymptotically as an equivalent inductance at higher frequencies. However, due to the impact of converter control dynamics, the phase angle goes outside the passive boundaries defined by $-90° < \theta < +90°$ in the region between 1.77 and 5 kHz. This is called the negative-resistive or non-passive area. It has to be noted that a negative-resistive behavior is equally observed in the DC-side equivalent admittance Y_{vsc}^{DC}, shown in Fig. 5b. In this case, the negative-resistive behavior appears in a frequency range between 1.7 and 5 kHz.

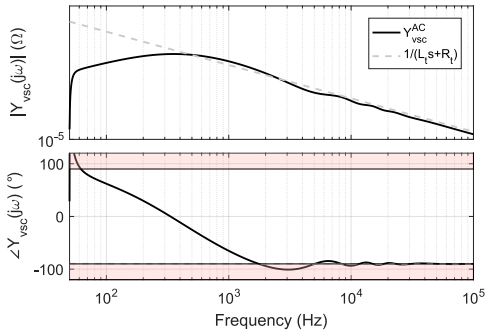

(a) AC side admittance

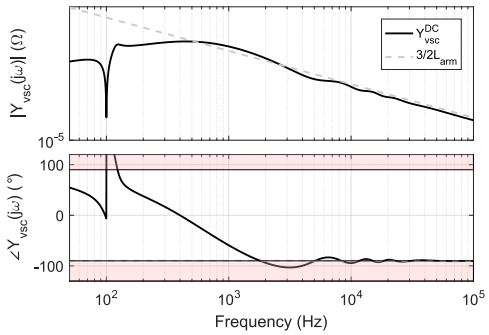

(b) DC side admittance

Fig. 5: MMC equivalent admittance representation considering control dynamics (solid) and only considering passive components (dashed) at the (a) AC and (b) DC side.

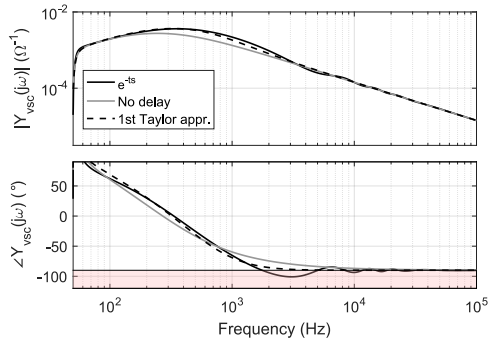

(a) AC side admittance

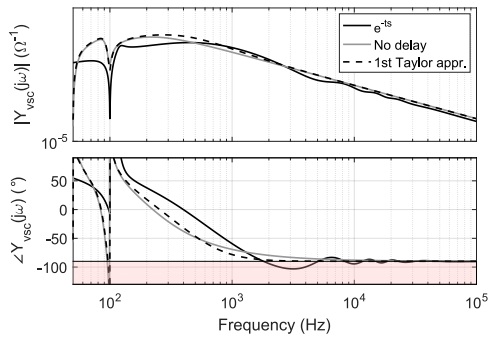

(b) DC side admittance

Fig. 6: MMC equivalent admittance with different dead-time representations at (a) the AC and (b) the DC side.

C. Impact of converter dead-time representation

This section investigates the impact of the converter dead-time representation on the equivalent converter impedance. In literature, the converter dead-time is often represented as a first order Taylor approximation, [2], given by (14) or even neglected [13].

$$e^{-t_d s} = \frac{1}{t_d s + 1}. \tag{14}$$

The main justification for this assumption lies in the negligible impact of this delay in the range of traditional power system stability studies at frequencies below the fundamental or within the controller bandwidth of the converter.

Fig. 6a shows the AC side converter admittance with the dead-time represented exactly by the exponential function, the first-order Taylor approximation and with the dead-time neglected. As observed, the representation of the dead-time has a significant impact on the equivalent MMC admittance in the kHz range. It is therefore suggested to use the exact exponential representation in order to get an accurate representation. A simplification of the dead-time representation results in a misleading capture of the actual negative-resistive equivalent response caused by the converter control dynamics. A similar influence is observed at the DC side converter admittance given in Fig. 6b.

D. Closed-loop system stability assessment method

Electromagnetic instability is characterized by the dynamic interaction between the converter, represented by the equivalent admittance Y^i_{vsc}, and the network represented by the equivalent impedance Z_i, with i indicating either the AC or DC side. One of the benefits of the impedance-based method is that only the frequency responses of the different system component are necessary to assess the system stability. This is graphically depicted in Fig. 7.

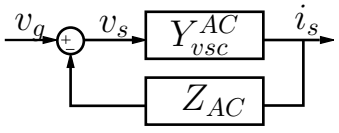

(a) AC side

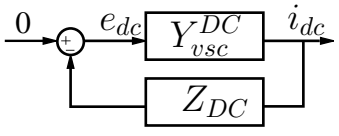

(b) DC side

Fig. 7: Closed-loop system stability representation.

At the AC side, the stability is analyzed using the feedback system in Fig. 7a, containing the equivalent converter AC admittance Y^{AC}_{vsc}, and the network dynamics represented by the equivalent impedance Z_{AC}. Similarly, for the DC system

stability analysis, the system is converted to a closed-loop representation of two transfer functions, Y_{vsc} and Z_{DC} (Fig. 7b). In this case, Y_{vsc} represents the DC side equivalent admittance of the DC voltage controlling MMC and gives the relation between DC voltage e_{dc} and current i_{dc}. The impedance Z_{DC} represents the remaining part of the link.

The electromagnetic stability can be assessed by means of the Nyquist stability criterion [14], [15]. In this paper, interactions are studied using the Bode plot of the loop-gain transfer functions, respectively $Y_{vsc}^{AC} Z_{AC}$ and $Y_{vsc}^{DC} Z_{DC}$, and by analysing the gain cross-over points and their phase margin, i.e, the points when the magnitude crosses 0 dB and the angle difference with -180°.

The different converter and network impedances at both sides can be obtained: (i) analytically by means of the use of linearized representations of components or (ii) applying a frequency sweep in the time-domain response and calculating the impedance from the FFTs of the calculated currents and voltages at the node of analysis. Both methods are implemented in the paper, illustrating the validity of both methods to study the electromagnetic stability.

IV. Study Case

A. AC side stability analysis

The test system for the AC side stability analysis is composed of a MMC converter with equivalent admittance Y_{vsc}^{AC} and an AC network with equivalent impedance Z_{AC}. The equivalent admittance is obtained by applying the MATLAB/Simulink *linmod* [16] function to the MMC model. Since the focus is on AC side interactions, the DC side is represented by a DC voltage source. The AC system corresponds to an overhead line of 25 km connected to an ideal voltage source. The transmission line is represented using the frequency-dependent parameter representation in the phase domain, which enables obtaining the equivalent impedance Z_{AC} of the AC grid.

The system stability is determined by the loop-gain transfer function of the interconnected system $Y_{vsc}^{AC} Z_{AC}$. Fig. 8 shows the Bode plot of $Y_{vsc}^{AC} Z_{AC}$. The gain cross-over points of the interconnected system are indicated by the red lines. Particularly at a frequency of 2180 Hz, $Y_{vsc}^{AC} Z_{AC}$ has a negative phase margin, thus indicating an electromagnetic instability.

This instability is confirmed by the time-domain simulation in EMTDC/PSCAD, where the converter is connected to the AC system at $t = 1.5$ s (Fig. 9) and the FFT applied to the time window of 20 ms after the disturbance. The relative error between the frequency determined from the analytical analysis and the PSCAD/EMTDC time-domain simulation is equal to 1.3 %.

B. DC side stability analysis

In this section, the impedance-based stability assessment is extended to the DC side of a VSC HVDC system. The VSC HVDC system consists of two MMCs, one controlling the DC voltage e_{dc} and the other one the active power P. The MMCs are connected with each other via DC overhead lines with a

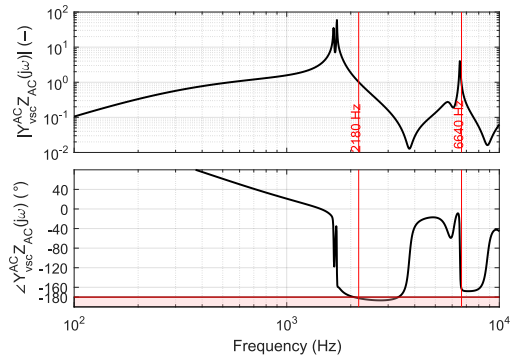

Fig. 8: Loop-gain transfer function $Y_{vsc}^{AC} Z_{AC}$.

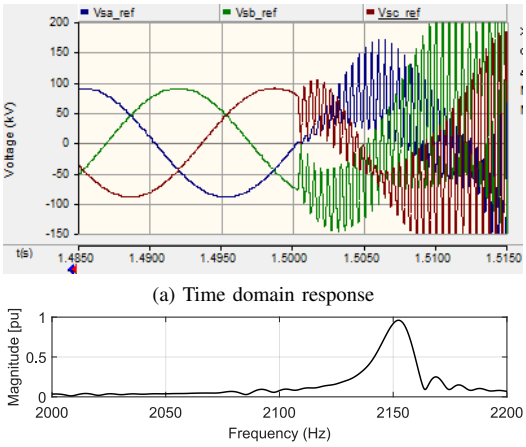

(a) Time domain response

(b) FFT

Fig. 9: Response of AC voltage at the PCC v_s, (a) in the time-domain, with (b) FFT (t=1.5-1.52 s).

length of 180 km. The model of the DC overhead line is based on [17]. The surrounding AC grid of Fig. 4 is represented by an ideal voltage source. In this case, the frequency responses of Y_{vsc}^{DC} and Z_{DC} are obtained by performing a frequency sweep on the VSC HVDC system model implemented in PSCAD/EMTDC, where Y_{vsc}^{DC} is the equivalent admittance of the DC voltage controlling MMC and Z_{DC} the equivalent impedance of the DC overhead lines combined with the active power controlling MMC. The Bode plot of the open-loop transfer function $Y_{vsc}^{DC} Z_{DC}$ is given in Fig. 10.

Similar to the AC side analysis, the stability of the system is assessed with the loop gain Bode plot. During the assessment, the active power demand of the VSC HVDC link is set to 0 and the DC voltage is controlled to 200 kV. In Fig. 11, the phase angle of Fig. 10 is closer observed in the kHz range. It is shown in Fig. 11 that at a frequency of 2960 Hz, when the magnitude equals 1, the phase angle is below the -180°-line which results in a negative phase margin. Hence, the impedance-based stability assessment predicts the instability of the VSC HVDC link for this configuration.

The prediction of the impedance-based stability assessment is confirmed by the time domain simulation performed on the

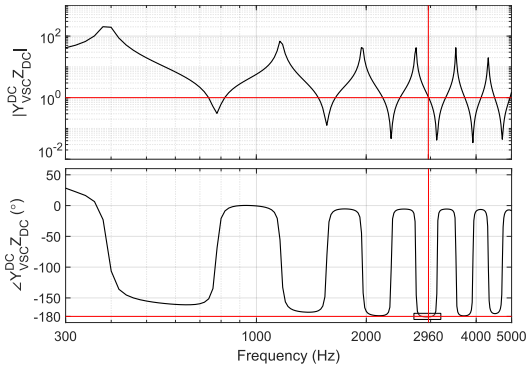

Fig. 10: Loop-gain transfer function $Y^{DC}_{vsc}Z_{DC}$.

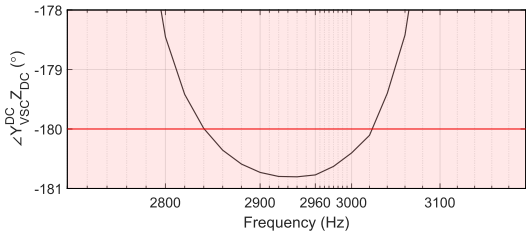

Fig. 11: Zoom in phase angle $Y^{DC}_{vsc}Z_{DC}$

VSC HVDC link model in PSCAD/EMTDC. Fig. 12 depicts the DC voltage e_{dc} as a function of the time. At t=1 s, when the two MMCs are in steady state, the two parts of the VSC HVDC link are connected. Immediately after the connection, a small oscillation appears in e_{dc}. This oscillation increases in an unstable way, resulting in unacceptable high values for the DC voltage e_{dc}. The zoom in of Fig. 12 shows an oscillation with a frequency of 2960 Hz. At this frequency, the magnitude value of $Y_{vsc}Z_{DC}$ is 0 dB and the phase angle is -180.6°.

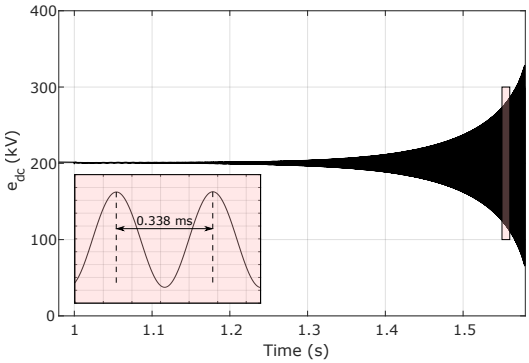

Fig. 12: Response of DC voltage e_{dc} in the time domain.

V. Conclusion

The analysis in this paper shows how electromagnetic instabilities cannot be excluded to take place at both the AC and DC side of a VSC HVDC link as a result of the interaction between the converter controllers and the electromagnetic characteristics of the connected electrical systems. Non-idealities in the control structures, such as the converter dead-time, cause non-passive regions in the converter equivalent admittance and make instabilities appear in the kHz range. Therefore, it is necessary to accurately represent both converter and network behavior over an extended frequency range to investigate the problem. The analysis shows how simplified dead-time representations fail in accurately capturing the dynamic converter behavior in the kHz range, and thereby do not allow assessing the problem accurately.

Acknowledgment

The research of Jef Beerten is funded by the Research Foundation – Flanders (FWO).

References

[1] C. Buchhagen, C. Rauscher, A. Menze, and J. Jung, "BorWin - First experiences with harmonics interactions in converter dominated grids," in *Proc. Int. ETG Congress 2015*, Bonn, Germany, Nov. 2015, 7 pages.

[2] H. Saad, Y. Fillion, S. Deschanvres, Y. Vernay, and S. Dennetiere, "On resonances and harmonics in HVDC-MMC station connected to AC grid," *IEEE Trans. Power Del.*, vol. 32, no. 3, pp. 1565–1573, 2017.

[3] H. Rao and S. Xu, "Operational experiences of Luxi BTB and Nao'ao MTDC projects in China," in *Proc. CIGRE B4 Colloquium*, Winnipeg, Canada, Oct.1–4, 2017.

[4] C. Rathke and M. Greeve, "Operating experience of HVDC links - Behaviour after switching events in the onshore grid," in *Proc. CIGRE B4 Colloquium*, Winnipeg, Canada, Oct.1–4, 2017.

[5] A. Bayo Salas, J. Beerten, and D. Van Hertem, "Analytical methodology to develop frequency-dependent equivalents in networks with multiple converters," in *Proc. IEEE PowerTech 2017*, Manchester, UK, Jun.18–22 2017.

[6] J. Beerten, S. D'Arco, and J. Suul, "Frequency-dependent cable modelling for small-signal stability analysis of VSC-HVDC systems," *IET Gener., Transm. Distrib.*, vol. 10, no. 6, pp. 1370–1381, 2016.

[7] H. Saad, "Performance analysis of INELFE link with control replicas [Accessed Apr. 24, 2018]," Aug. 2016. [Online]. Available: http://sites.google.com/site/hvdcreplicaworkshop/workshop-presentations

[8] G. Pinares, "On the analysis of DC network dynamics of VSC-based HVDC systems," Licentiate of engineering, Chalmers University of Technology, 2014.

[9] G. Stamatiou, "Converter interactions in VSC-based HVDC systems," Licentiate of engineering, Chalmers Univeristy of Technology, 2015.

[10] K. Sharifabadi, L. Harnefors, H.-P. Nee, S. Norrga, and R. Teodorescu, *Design, control, and application of modular multilevel converters for HVDC transmission systems*, J. Wiley and Sons, Eds., 2016.

[11] H. Saad, J. Peralta, S. Dennetiere, J. Mahseredjian, J. Jatskevich, J. Martínez, A. Dovoudi, M. Saeedifard, V. Sood, X. Wang, J. Cano, and A. Mehrizi-Sani, "Dynamic averaged and simplified models for MMC-based HVDC transmission systems," *IEEE Trans. Power Del.*, vol. 28, no. 3, pp. 1723–1730, 2013.

[12] N. Ahmed, L. Ängquist, S. Norrga, A. Antonopoulos, L. Harnefors, and H.-P. Nee, "A computationally efficient continuous model for the modular multilevel converter," *IEEE Trans. Emerg. Sel. Topics Power Electron.*, vol. 2, no. 4, pp. 1139–1148, 2014.

[13] L. P. Kunjumuhammed, C. P. Bikal, C. Oates, and K. J. Dyke, "Electrical ocillations in wind farm systems: analysis and insight based on detailed modeling," *IEEE Trans. Sustain. Energy*, vol. 7, no. 1, pp. 51–62, 2016.

[14] L. Harnefors, M. Bongiorno, and S. Lundberg, "Input-admittance calculation and shaping for controlled voltage-source converters," *IEEE Trans. Ind. Electron.*, vol. 54, no. 6, pp. 3323–3334, 2007.

[15] J. Sun, "Impedance-based stability criterion for grid-connected inverters," *IEEE Trans. Power Electron.*, vol. 26, no. 11, pp. 3075–3078, 2011.

[16] Mathworks Inc., *Matlab user manual*, 2016.

[17] Z.-Y. He, K. Liao, X. P. Li, S. Lin, J.-W. Yang, and R.-K. Mai, "Natural frequency-based line fault location in HVDC lines," *IEEE Trans. Power Del.*, vol. 29, no. 2, pp. 851–859, 2014.